AIMS Materials Science, 10(6): 948–964.
DOI: 10.3934/matersci.2023051
Received: 19 March 2023
Revised: 24 September 2023
Accepted: 07 October 2023
Published: 26 October 2023

http://www.aimspress.com/journal/Materials

Research article

Study of ordering in 2D ferromagnetic nanoparticles arrays: Computer simulation

Sergey V. Belim*

Department of Physics, Omsk State Technical University, 11 pr. Mira, Omsk 644050, Russia

* **Correspondence:** Email: sbelim@mail.ru.

Abstract: This article describes ordering in a 2D ferromagnetic nanoparticles array by computer simulation. The Heisenberg model simulates the behavior of spins in nanoparticles. Nanoparticles interact using dipole-dipole forces. Computer simulations use the Monte Carlo method and Metropolis algorithm. Two possible types of ordering for the nanoparticles' magnetic moments are detected in the system. The magnetic anisotropy direction for the nanoparticles determines the type of ordering. If the anisotropy direction is oriented perpendicular to the substrate plane, then a superantiferromagnetic phase with staggered magnetization is realized. If the magnetic anisotropy is oriented in the nanoparticle plane, the superantiferromagnetic phase has a different structure. The nanoparticle array is broken into chains parallel to the anisotropy orientations. In one chain of nanoparticles, magnetic moments are oriented in the same way. The magnetic moments of the nanoparticles are oriented oppositely in neighbor chains. The temperature of phase transitions is calculated based on finite dimensional scaling theory. Temperature depends linearly on the intensity of the dipole-dipole interaction for both types of superantiferromagnetic transition.

Keywords: ferromagnetic nanoparticles array; antiferromagnetic; phase transition; dipole-dipole interaction; computer simulation

1. Introduction

2D arrays of ferromagnetic nanoparticles are promising materials with controllable magnetic properties. Nanoparticle films are used in spintronic devices. Experimentally, 2D nanoparticle arrays are made by deposition from a liquid medium onto a structured substrate [1,2] or lithographic division

of a thin film into isolated regions [3,4]. Both methods control particle sizes and their relative positions. Changing the structure of the substrate determines the shape and size of the particles. The lithographic method creates the most ordered arrays of nanoparticles. The same size of the nanoparticles provides their same magnetic moments below the blocking temperature [5].

The magnetic properties of the individual nanoparticles differ from the bulk materials. Nanoparticles are single-domain due to their small size. There is no phase transition in the individual nanoparticle. There is a blocking temperature below which the nanoparticles have a non-zero magnetic moment. Collective phenomena in nanoparticle arrays lead to new magnetic properties. The system enters a superparamagnetic state at a temperature below the blocking temperature in the absence of interaction between the nanoparticles. The magnetic moments of the nanoparticles are oriented differently in this phase. The interaction between the magnetic moments of the nanoparticles leads to superordered phases in the system. The interaction between the nanoparticles may be exchangeable or dipole-dipole. The exchange interaction dominates if the distance between nanoparticles is small. It is energetically advantageous for the magnetic moments of the nanoparticles to have the same direction in this case. Exchange interaction leads to the implementation of the superferromagnetic phase [5–8]. Monte Carlo computer modeling within the Ising model showed that the phase transition temperature in such systems depends on the intensity of interaction between nanoparticles by logarithmic law [9].

Dipole-dipole forces dominate if the distance between particles is large enough for an exchange interaction. The distance should not be very large, since the dipole-dipole forces decrease with the distance according to the power law. Dipolar interaction can lead to different types of ordering. A weak dipole-dipole interaction can create a superspin glass state. This collective ordering is analogous to atomic spin glasses [10]. Increased dipolar interaction can result in superferromagnetic phase [11]. Confirmation of this condition was obtained experimentally on granular films [12–15]. The interaction between nanoparticles depends on the distance between them. The lattice period of the nanoparticles can be controlled in metamaterials, which are non-magnetic matrices with periodically placed nanoparticles. These states are described within the mean field theory [16]. Computer modeling of a nanoparticle array with a dipole-dipole interaction within the Ising model demonstrated that superantiferromagnetic ordering of particle superspins can be realized in the system [17]. The phase transition temperature also depends on the interaction intensity by logarithmic law.

The Ising model describes particles with a light magnetizing axis. The Heisenberg model with the anisotropy axis is more adequate for real magnetic nanoparticles. The complex interaction between single-particle anisotropy and interparticle interaction should be taken into account when describing the magnetic behavior of the nanoparticle array. The effects of single-particle anisotropy and interparticle interaction have been experimentally investigated in various papers [18–23]. The dipolar interaction energy can have both positive and negative values depending on the direction of the nanoparticle anisotropy axes. The sign of energy depends on the mutual orientation of the nanoparticle superspins. Dipole-dipole forces can orient nanoparticle magnetizations in both one and different directions.

The purpose of this study is to investigate possible types of ordering of 2D arrays of ferromagnetic nanoparticles within the Heisenberg model with the anisotropy axis.

2. Model and methods

A computer experiment investigates a 2D array of ferromagnetic nanoparticles. Nanoparticles are located in the nodes of the square grid. The distance between the nanoparticles equals *d*. Nanoparticles are located in the *OXY* plane with equation z = 0. Nanoparticles have the size $a \times a \times a$ atoms. Periodic boundary conditions apply to the system along the *OX* and *OY* axes to eliminate the effects of system limitations. The geometry of the system is shown in Figure 1.

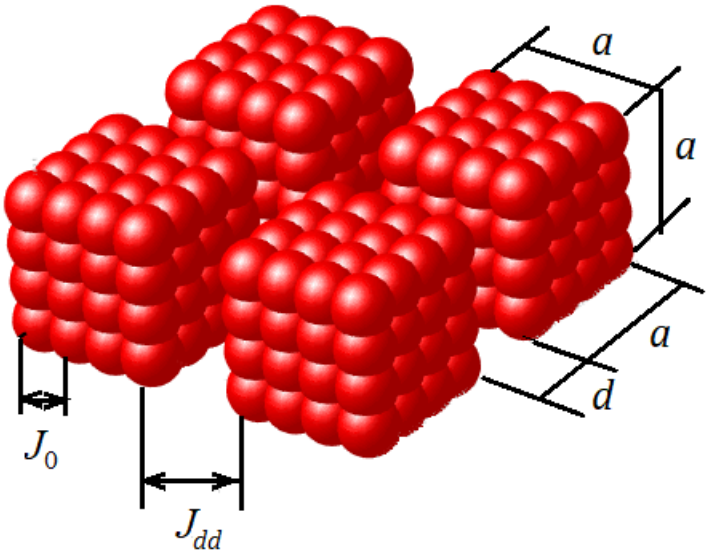

Figure 1. The geometry of the system. *a* is the size of a single nanoparticle. *d* is the distance between neighboring nanoparticles. J_0 is an exchange integral within a nanoparticle. J_{dd} is the intensity of the dipole-dipole interaction between neighboring nanoparticles.

Each atom has spin $\vec{S} = (S_x, S_y, S_z)$, $|\vec{S}| = 1/2$. Heisenberg's model describes such a spin system. The Hamiltonian of the Heisenberg model is the sum of the pair interactions for the nearest neighbors (Eq 1).

$$H = \sum J(\vec{S}_i, \vec{S}_j) \tag{1}$$

The spins $\vec{S}_i$ and $\vec{S}_j$ are located in neighbor nodes. The interaction type depends on the location of the spins. A pair of spins in one nanoparticle interact using exchange forces. Pairs of spins from neighbor nanoparticles interact with dipole-dipole forces. Exchange interaction includes two terms (Eq 2).

$$J(\vec{S}_i, \vec{S}_j) = -J_0 \vec{S}_i \vec{S}_j - A(\vec{S}_i, \vec{S}_j) \tag{2}$$

The second term takes into account the energy of anisotropy. The exchange integral equals J_0. Exchange forces rapidly decrease with distance. The exchange interaction between the nanoparticles will be small with a large distance between them. Dipole-dipole forces act between the spins of

neighbor particles. The dipole-dipole interaction has greater intensity than the exchange interaction for spins from neighbor particles. The dipole-dipole forces energy $J_{dd}(\vec{S}_i, \vec{S}_j)$ determines the interaction of spins in this case. The energy of the dipole-dipole interaction depends on the orientation of the spins relative to the radius vector r of their connecting (Eq 3).

$$J(\vec{S}_i, \vec{S}_j) = J_{dd}(\vec{S}_i, \vec{S}_j) = B\frac{(\vec{S}_i\vec{S}_j)r_{ij}^2 - 3(\vec{S}_i\vec{r}_{ij})(\vec{S}_j\vec{r}_{ij})}{r_{ij}^5} \tag{3}$$

$\vec{r}_{ij}$ is the radius vector between the spins $\vec{S}_i$ and $\vec{S}_j$. B is the dipole forces intensity. Dipole-dipole forces act between the spins of neighbor nanoparticles at a distance d. The dipole interaction energy is written in simplified form (Eq 4).

$$J_{dd}(\vec{S}_i, \vec{S}_j) = B\frac{(\vec{S}_i\vec{S}_j) - 3\vec{S}_{id}\vec{S}_{jd}}{d^3} \tag{4}$$

$\vec{S}_{id}$ and $\vec{S}_{jd}$ are projections of the spins $\vec{S}_i$ and $\vec{S}_j$ onto the radius vectors between them. The intensity of dipole-dipole interaction between nanoparticles is calculated relative to the exchange interaction within the nanoparticle (Eq 5).

$$R = \frac{B}{J_0 d^3} \tag{5}$$

Relative values are more convenient in computer simulations. The computer experiment uses the formula for dipole-dipole interaction energy with relative values (Eq 6).

$$J_{dd}(\vec{S}_i, \vec{S}_j) = RJ_0\left((\vec{S}_i\vec{S}_j) - 3\vec{S}_{id}\vec{S}_{jd}\right) \tag{6}$$

The value R depends on the substance of the nanoparticles and the distance between them. The computer experiment uses different values of R. The increase in R corresponds to a decrease in the distance between the nanoparticles.

The exchange interaction makes it advantageous to orient the spins in one direction. The dipole-dipole interaction can order spins in both one direction and different directions. The orientation and magnitude of anisotropy are important in the type of spin ordering. A computer experiment is performed for two cases of anisotropy orientation. The direction of anisotropy for all nanoparticles is the OZ axis in the first case. The direction of anisotropy is perpendicular to the nanoparticle plane in this case. The anisotropy term in Eq 2 depends on the projection of the spins $\vec{S}_i$ onto the OZ axis S_i^z (Eq 7).

$$A(\vec{S}_i, \vec{S}_j) = KS_i^z S_j^z \tag{7}$$

The anisotropy parameter K depends on the kind of substance. The computer experiment uses a value $K = 0.63\,J_0$. This value is characteristic for some materials [24–26].

The anisotropy direction determines the preferential spin's orientation. If the OZ axis is the anisotropy direction, then the spin's projection onto the OZ axis dominates the rest of the directions. The particles' spins are oriented substantially perpendicular to the radius vector between the nanoparticles (Eq 8).

$$J_{dd}(\vec{S}_i, \vec{S}_j) = RJ_0(\vec{S}_i\vec{S}_j) \tag{8}$$

As a result, the dipole-dipole interaction energy has a positive value for co-directed spins and a negative value for oppositely directed spins. It is energetically advantageous for neighbor nanoparticles to have oppositely directed magnetic moments. The dipole-dipole interaction results in a superantiferromagnetic phase in the nanoparticle array.

Staggered magnetization of nanoparticles describes the transition to a superantiferromagnetic state. The nanoparticle magnetic moment $\vec{m}_{lk} = (m_{lkx}, m_{lky}, m_{lkz})$ is equal to the average value of the spins of atoms in the nanoparticle with coordinates (l, k) (Eq 9).

$$\vec{m}_{lk} = \left(\sum_{S_i \in m_{lk}} \vec{S}_i \right) \Big/ a^3 \tag{9}$$

a is the size of the nanoparticle.

Staggered magnetization $\vec{m}$ is equal to difference of magnetic moments in two nanoparticle sublattices (Eq 10).

$$\vec{m} = \left(\sum_{\substack{l,k=1 \\ l+k=even}}^{L} \vec{m}_{lk} - \sum_{\substack{l,k=1 \\ l+k=odd}}^{L} \vec{m}_{lk} \right) \Big/ L^2 \tag{10}$$

L is the number of nanoparticles along one axis.

The anisotropy direction for particles is the OX axis in the second case. The anisotropy direction lies in the plane of the particles. The anisotropy term in Eq 2 is determined by the projection of the spins $\vec{S}_i$ onto the OX axis S_i^x (Eq 11).

$$A(\vec{S}_i, \vec{S}_j) = KS_i^x S_j^x \tag{11}$$

The dipole-dipole interaction has a different sign for different particle arrangements (Figure 2).

The dipole-dipole interaction energy J_{ddx} is negative at co-directional magnetic moments for particles located along a straight parallel *OX* axis (Eq 12).

$$J_{ddx}(\vec{S}_i, \vec{S}_j) = -2RJ_0(\vec{S}_i\vec{S}_j) \tag{12}$$

The dipole-dipole interaction energy J_{ddy} for particles with oppositely directed magnetic moments is negative if the particles are adjacent along the OY axis (Eq 13).

$$J_{ddy}(\vec{S}_i, \vec{S}_j) = RJ_0(\vec{S}_i\vec{S}_j) \tag{13}$$

Ordering the magnetic moments of nanoparticles in one direction is energetically advantageous for chains of particles oriented along the OX axis. The magnetic moments of neighbor nanoparticle chains are oriented oppositely (Figure 3).

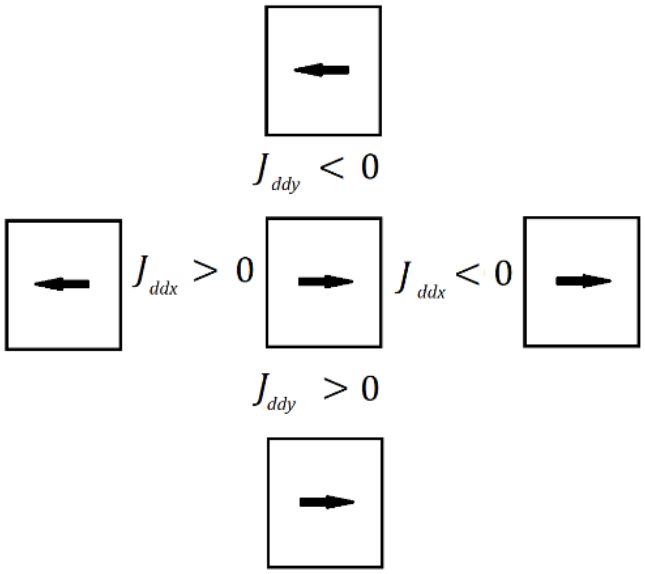

Figure 2. Dipole-dipole interaction energy at different orientation of nanoparticle magnetization. Arrows show the direction of magnetization of the nanoparticle. The sign of the dipole-dipole interaction is indicated between each pair of nanoparticles. J_{ddx} is the dipole-dipole interaction energy of *OX*-adjacent nanoparticles. J_{ddy} is the dipole-dipole interaction energy of *OY*-adjacent nanoparticles.

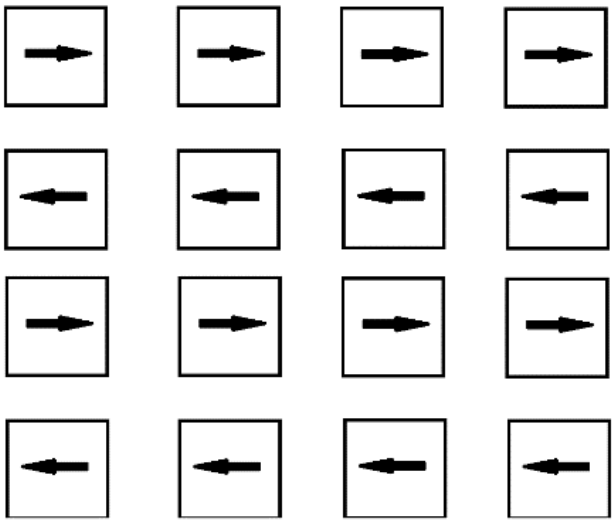

Figure 3. Chains of particles ordered by dipole-dipole interaction. Arrows show the direction of magnetization of the nanoparticle.

Another type of superantiferromagnetic ordering is realized in this case. The order parameter for such a phase $\vec{m}_a$ is equal to the magnetization difference of the sublattices. Each sublattice is a set of nanoparticle chains oriented along the OX axis. Nanoparticles of the first sublattice have even numbers along the OY axis. Nanoparticles of the second sublattice have odd numbers along the OY axis (Eq 14).

$$\vec{m}_a = \left(\sum_{k=odd} \vec{m}_{lk} - \sum_{k=even} \vec{m}_{lk} \right) / L^2 \tag{14}$$

Such a superantiferromagnetic phase is called a chain phase.

The structure of the chain phase is similar to the structure of layered antiferromagnets. The dimension of the layers is one. This structure imposes a limitation on computer simulations. Dimensions of system L along axes OX and OY shall be even. In this case, the superspins are oriented oppositely at opposite edges of the system. If the size L is odd, then periodic boundary conditions result in the same orientation directions of the superspin chains at the system boundary. As a result, the system becomes frustrated. The stationary phase is not present in such a system. This is a feature of the model, not the real physical system. Proper sizing in system modeling eliminates problems. The even system size requirement is also imposed at the superantiferromagnetic phase. If the system size is odd, periodic boundary conditions result in a frustrated state of the superspin system.

3. Computer simulation

The Metropolis algorithm [27] simulates the states of system spins at different temperatures. The number of Monte Carlo steps per spin is 8×10^6.

The modeling algorithm is modified to take into account the division of the system into nanoparticles. All spins are directed randomly in the initial state. At each step, the algorithm selects a random nanoparticle and attempts to rotate the spin of the nanoparticle alternately. The spins at the nanoparticle boundary turn first. After that, the algorithm moves to the center of the nanoparticle. This approach takes into account the single-domain nature of nanoparticle magnetization.

Phase transitions of the second kind occur only in infinite systems. The algorithm uses periodic boundary conditions and finite-dimensional scaling theory to level the finite dimensions of simulated systems. Finite-dimensional scaling theory [27] provides a method for determining the phase transition temperature in a computer experiment. A computer experiment simulates systems with different linear sizes $L \times L$. System dimensions take values from $L = 8a$ to $L = 16a$ with step $\Delta L = 2a$. a is the size of a single nanoparticle. Fourth order Binder cumulants $U(L,T)$ [28] are calculated for each system at different temperatures (Eq 15).

$$\begin{gathered} U(L,T) = 1 - \frac{\langle m^4 \rangle}{3\langle m^2 \rangle^2}, m^2 = m_x^2 + m_y^2 + m_z^2 \\ U_a(L,T) = 1 - \frac{\langle m_a^4 \rangle}{3\langle m_a^2 \rangle^2}, m_a^2 = m_{ax}^2 + m_{ay}^2 + m_{az}^2 \end{gathered} \tag{15}$$

Angle brackets denote averaging over thermodynamic configurations. The Binder cumulant does not depend on the size of the system at the phase transition temperature according to finite-dimensional scaling theory. Binder cumulant temperature plots for systems with different sizes intersect at a single point. This point corresponds to the phase transition temperature.

The dependence of Binder cumulants on temperature for systems with different sizes is shown in Figure 4.

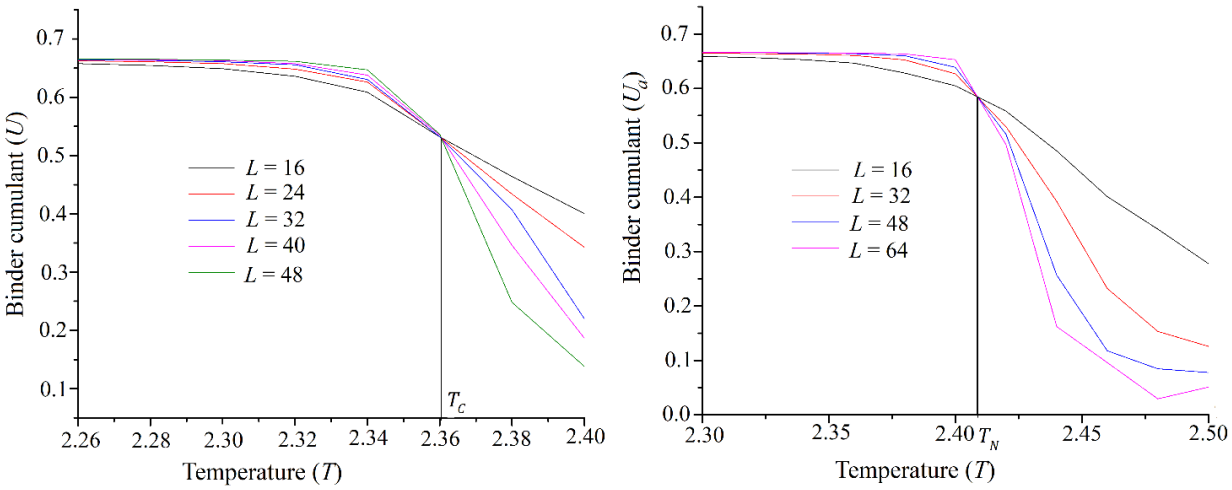

(a) (b)

Figure 4. Temperature dependence of Binder cumulants for systems with different sizes. (a) Anisotropy axis is parallel to OZ axis ($a = 8,\ R = 0.7$). (b) Anisotropy axis is parallel to OX axis ($a = 8,\ R = 0.7$). The temperature T is given in relative units.

Finite dimensional scaling theory allows one to calculate the behavior of various thermodynamic functions. Magnetic susceptibility is calculated based on the average value of the order parameter (Eq 16).

$$\chi = \frac{\partial m}{\partial h} = \frac{NJ}{T}(\langle m^2\rangle - \langle m\rangle^2)$$
$$\chi_a = \frac{\partial m_a}{\partial h} = \frac{NJ}{T}(\langle m_a^2\rangle - \langle m_a\rangle^2) \quad (16)$$

In this case, the complex magnetic susceptibility of nanoparticle sublattices is calculated. Magnetic susceptibility exhibits singular behavior near the phase transition temperature. Examples of dependence plots for magnetic susceptibility for nanoparticles with size $a = 8$ and dipolar interaction intensity $R = 0.7$ are shown in Figure 5.

The dependence of susceptibility on temperature near the critical point is approximated by the power function (Eq 17).

$$\chi \sim |T - T_C|^{-\gamma}, \chi_a \sim |T - T_N|^{-\gamma_a} \quad (17)$$

γ and γ_a are critical exponents. Finite-dimensional scaling theory determines the dependence of thermodynamic functions on the size of the system (Eq 18).

$$\chi \sim L^{\gamma/\nu}, \chi_a \sim L^{\gamma_a/\nu_a} \quad (18)$$

ν and ν_a are critical exponents describing the growth of the correlation radii γ and γ_a near the critical temperature (Eq 19).

$$r \sim |T - T_C|^{-\nu}, r_a \sim |T - T_N|^{-\nu_a} \quad (19)$$

Finite-dimensional scaling theory incorporates these critical exponents into the behavior of Binder cumulants when changing the size of a system at critical temperature (Eq 20).

$$\frac{\partial U}{\partial T} \sim L^{1/\nu}, \frac{\partial U_a}{\partial T} \sim L^{1/\nu_a} \tag{20}$$

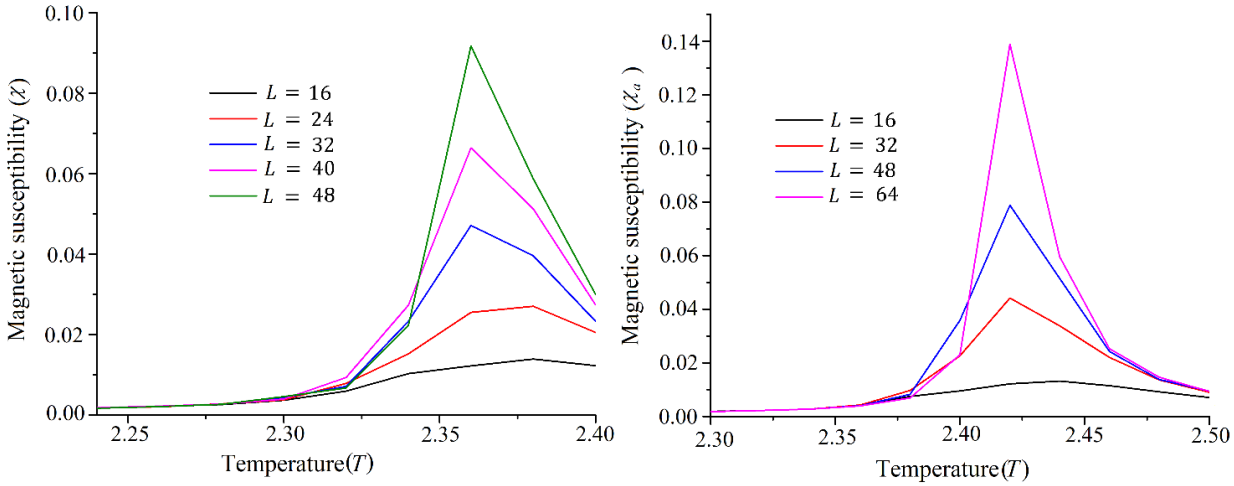

(a) (b)

Figure 5. Examples of dependence plots for magnetic susceptibility for nanoparticles with size $a = 8$ and dipolar interaction intensity $R = 0.7$. (a) Nanoparticles with direction of anisotropy along OZ axis. (b) Nanoparticles with direction of anisotropy along OX axis. The temperature T is given in relative units.

Plots for the dependence of derivatives $\partial U/\partial T$ and $\partial U_a/\partial T$ on the size of the system L on a logarithmic scale at critical temperature make it possible to find critical exponents ν and ν_a. Plots for the dependence of susceptibility χ and χ_a on the size of the system L at critical temperature on a logarithmic scale make it possible to determine the ratios of critical exponents γ/ν and γ_a/ν_a.

The dependence of order parameters on the temperature near the phase transition is also described by the power function (Eq 21).

$$m \sim |T - T_C|^{\beta}, m_a \sim |T - T_N|^{\beta_a} \tag{21}$$

Finite-dimensional scaling theory describes the dependencies of order parameters on system dimensions (Eq 22).

$$m \sim L^{-\beta/\nu}, m_a \sim L^{-\beta_a/\nu_a} \tag{22}$$

Plots for the dependence of order parameters on the dimensions of the system at critical temperature on a logarithmic scale allow one to find the ratio of critical exponents β/ν and β_a/ν_a.

Critical exponents can be calculated from plots of thermodynamic functions versus temperature. To do this, it is necessary to know the exact value of the phase transition temperature. This temperature can be determined from the peak of the magnetic susceptibility plot. However, the position of the peak in the graph is determined up to temperature step in the algorithm. This inaccuracy leads to large errors in the definition of critical exponents. A small error in determining

the phase transition temperature leads to significant errors in the critical exponents. Finite dimensional scaling theory makes it possible to more accurately determine the temperature of the phase transition from Binder cumulants. Binder cumulants do not exhibit singular behavior and are smooth functions. The approximation of Binders cumulants allows one to obtain their values with high accuracy. Scale ratios for thermodynamic functions depending on the size of the system give good values for critical exponents. It should be noted that the critical temperature obtained from Binder cumulants has a lower value than the temperature based on the magnetic susceptibility peak. This pattern is observed for all spin models.

4. Results

The first computer experiment examines a nanoparticles array with the anisotropy direction along the OZ axis. The phase transition temperature depends on the size of the nanoparticles a and the relative intensity of the dipole-dipole interaction R. The Neel temperature T_C is calculated for different values of the dipole-dipole interaction relative intensity from $R = 0.3$ to $R = 0.7$ in steps $\Delta R = 0.1$. The Neel temperature T_C dependence on the dipole-dipole interaction intensity R for the three nanoparticle sizes is demonstrated in Figure 6.

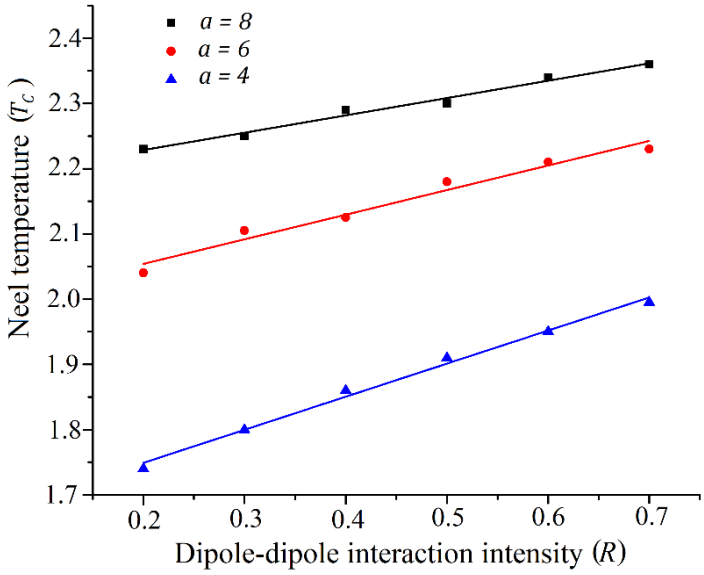

Figure 6. The Neel temperature T_C dependence on the dipole-dipole interaction intensity R for the three nanoparticle sizes. The temperature T_C is given in relative units. The temperature T is given in relative units.

Neel temperature increases linearly with increasing intensity of the dipole-dipole interaction. This result is associated with an increase in the total energy ordering the spins. The phase transition temperature decreases as the size of the nanoparticles decreases. This pattern is due to the increasing role of the dipole-dipole interaction in the ordering of spins. The dipole-dipole interaction has a lower intensity compared to the exchange interaction. The contribution of the dipole-dipole interaction to the total energy increases as the particle size decreases. Small particles have fewer

pairs of spins interacting with exchange forces. The phase transition temperature is determined by the average thermal energy required to flip the individual spin. Spin reversal is hindered by spin-spin interaction. As the spin-spin interaction decreases, the phase transition temperature decreases.

This ordering comes from the superparamagnetic phase to the superantiferromagnetic phase. The particles individually enter an ordered state at a higher temperature. The ordering of spins in a single particle occurs at the blocking temperature T_B. The particle blocking temperature is higher than the system Neel temperature ($T_B > T_C$). The mean absolute value of magnetic moments for nanoparticles describes magnetization without considering the orientation of magnetic moments (Eq 23).

$$m_p = \sum_{l,k=1}^{L} |\vec{m}_{lk}| \Big/ L^2 \tag{23}$$

$|m_{lk}|$ is the magnetization module of the nanoparticle with coordinates(l,k). m_p takes a value 1/2 if the spins within each nanoparticle are ordered. Magnetization of different particles can be directed in different directions. The superparamagnetic phase is realized in this case. The dependence of the staggered magnetization in the system m and mean absolute value of magnetic moments m_p on the temperature T for the system with $L = 16$ nanoparticles of size $a = 8$ at $R = 0.5$ are shown in Figure 7.

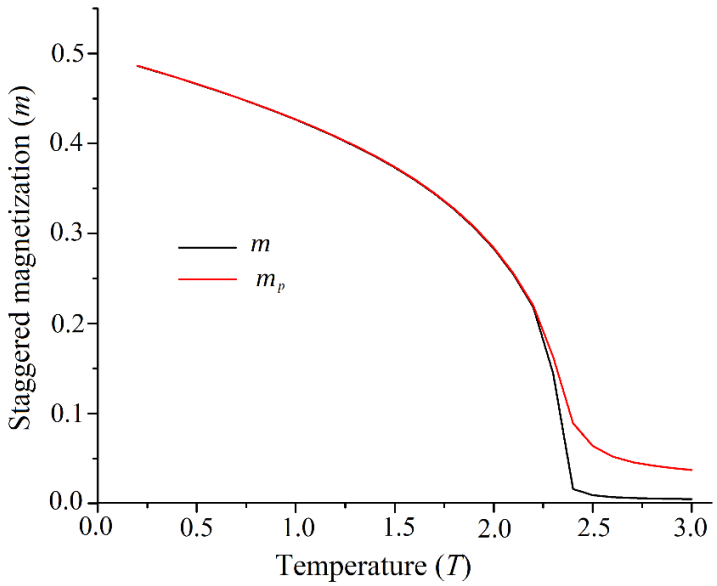

Figure 7. The dependence of the staggered magnetization in the system m and mean absolute value of magnetic moments m_p on the temperature T for the system with $L = 16$ nanoparticles of size $a = 8$ at $R = 0.5$. The temperature T is given in relative units.

Staggered magnetization in system m and mean absolute value of magnetic moments m_p coincide at temperature below Neel temperature ($T < T_C$). At temperatures above the phase transition temperature ($T > T_C$), the staggered magnetization in the system decreases rapidly. The mean absolute value m_p remains non-zero over a large temperature range. These values indicate a

superparamagnetic phase. Magnetic moments in nanoparticles are oriented in different directions. The checkerboard magnetization in the system is zero $m = 0$. The inequality $m_p > m$ is performed in the superparamagnetic phase. Nanoparticles are single-domain due to their small size. The transition from a fully disordered phase to a superparamagnetic phase is not a phase transition.

A second computer experiment examines an array of nanoparticles with the anisotropy direction along the OX axis. The plots for the dependence of the order parameter m_a and mean absolute value of magnetic moments m_p on temperature T are shown in Figure 8.

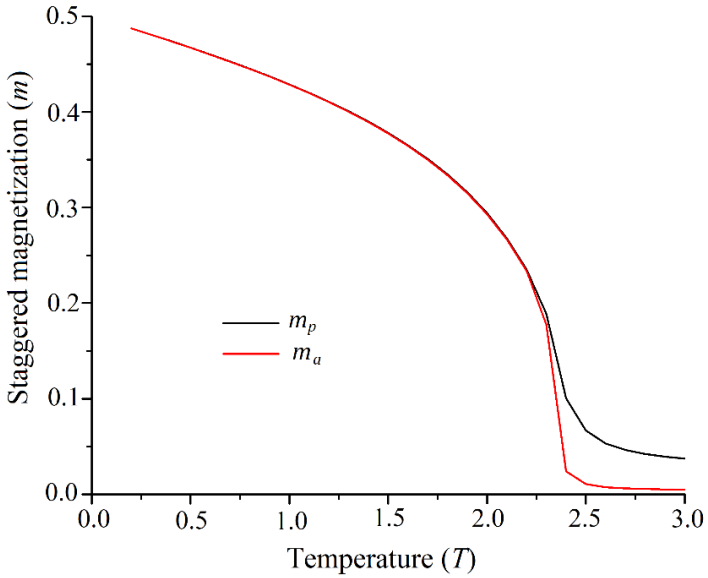

Figure 8. Plots for the dependence of the order parameter m_a and mean absolute value of magnetic moments m_p on temperature T at $a = 8$, $L = 16$ and $R = 0.5$. The temperature T is given in relative units.

Chain ordering comes from the superparamagnetic phase as well as in the anisotropy orientation along the OZ axis. Plots for the Neel T_N chain-ordered temperature versus dipole-dipole interaction intensity R for particles with different sizes a are shown in Figure 9.

The Neel temperature of T_N for chain ordering increases linearly with increasing intensity of the dipole-dipole interaction R. This trend is attributed to the increasing interaction between nanoparticles. The phase transition temperature T_N increases with increasing particle size a. This growth is due to the fact that more pairs of spins interact through an exchange interaction. The exchange interaction has a higher intensity than the dipole-dipole interaction.

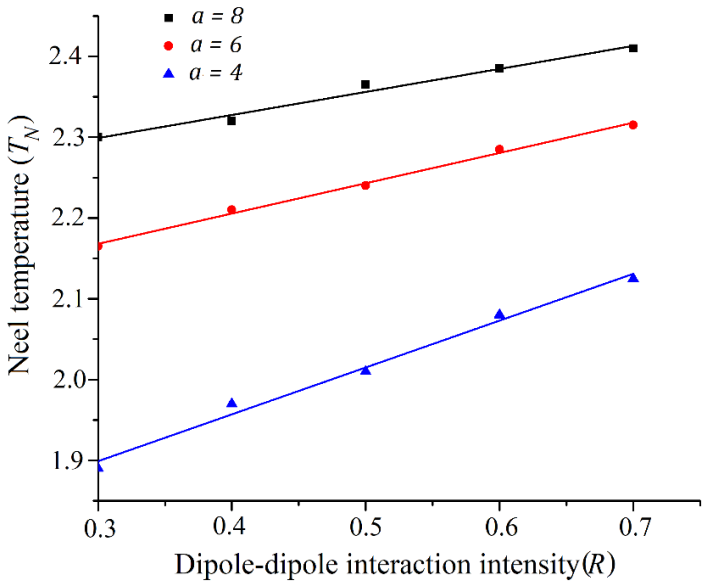

Figure 9. Plots for the Neel T_N chain-ordered temperature versus dipole-dipole interaction intensity R for particles with different sizes a. The temperature T is given in relative units.

5. Conclusions

Computer simulations of the 2D nanoparticle array exposed the possibility for two types of superantiferromagnetic ordering. The type of ordering depends on the orientation of the nanoparticle anisotropy axis. If the nanoparticle anisotropy axis is directed perpendicular to the plane of the system substrate, then staggered ordering is realized. If the anisotropy axis of the nanoparticles lies in the plane of the substrate, then the system is divided into two sublattices. Each sublattice is a set of parallel nanoparticles chains. The nanoparticle chains are oriented along the direction of the anisotropy axis.

Modern methods of nanoparticle synthesis allow controlling their anisotropy [29,30]. Anisotropy can be realized in the particle production step. The anisotropy direction can also change under the influence of external factors. The effective anisotropy of nanoparticles can change under the influence of temperature and their concentration [31]. A transition from one type of superantiferromagnetic ordering to another is possible when the direction of nanoparticle anisotropy changes.

Superantiferromagnetic ordering has been experimentally observed in various systems. An array of Co nanocrystals on a carbon substrate with a particle size 12 nm demonstrates a transition from a superparamagnetic phase to a superantiferromagnetic one [32]. The ordering type varies at temperatures below 300 K. Nanoparticles in this system have high anisotropy. ZnO nanoparticles show similar types of ordering on different substrates at room temperatures [33–39]. Experimental study of the behavior for Fe/Fe_3O_4 nanoparticles on the CoFeB surface demonstrated the dependence of the phase transition temperature on the intensity of interaction between particles [40].

This article discusses systems with a sufficiently large value of the anisotropy constant. With smaller values of this constant, it is possible to magnetize nanoparticles in directions that do not coincide with the anisotropy axis. Collective ordering is possible in systems with chaotically oriented anisotropy axes of individual nanoparticles. The phase diagram of such systems requires additional research.

Calculations of critical exponents show their independence from the intensity of the dipole-dipole interaction R. Also, critical exponents are independent from the size of nanoparticles a. Critical exponents are equal to $\nu = 1.00 \pm 0.04$, $\gamma = 1.78 \pm 0.02$, $\beta = 0.10 \pm 0.03$. These values are close to the critical exponents of thin films [41].

Only one value of the anisotropy parameter is used when simulating the system. The behavior of the system does not change qualitatively when the value of the anisotropy parameter varies. The absence of anisotropy leads to the impossibility of an ordered phase at temperatures other than zero ($T > 0$). If the anisotropy parameter is much less than the exchange interaction constant, then the ordering of the nanoparticles magnetic moments does not occur. The minimum value of the anisotropy parameter required for the appearance of a super-ordered phase requires additional investigation.

Changing the direction of effective nanoparticle anisotropy also requires additional modeling. If the angle between the direction of anisotropy and the OZ axis changes under the action of external parameters, then the superantiferromagnetic phase passes into the chain phase. The type of this phase transition should be studied further. It can be expected to be similar to the spin-flop transition. For such a transition, there must be a critical angle of direction of anisotropy, which leads to a change in the type of superantiferromagnetic ordering.

The behavior of an array of ferromagnetic nanoparticles with dipolar interaction in an external magnetic field also remains unexplored. The magnetic field suppresses the antiferromagnetic phase in ordinary substances. There is a critical value for the strength of the external magnetic field, above which antiferromagnetic ordering is replaced by ferromagnetic ordering. The same pattern should exist for superantiferromagnetic ordering of the nanoparticle's magnetic moments. This process will be more complex in an array of dipolar interaction nanoparticles. Two additional factors will influence the change in ordering type. The magnetization of nanoparticles is more difficult than the rotation of a single spin. The critical strength will depend on the angle between the direction of the magnetic field and the anisotropy axis of the nanoparticles. The process of suppressing the superantiferromagnetic phase and the chain phase will differ.

Artificial spin ice is formed from arrays of nanoparticles. A necessary condition for the existence of spin ice is the presence of long-range anisotropic magnetic interactions between nanoparticles. The model proposed in this paper does not show the state of spin ice. This phase requires additional assumptions in the model. Obtaining spin ice in an array of nanoparticles is the task of the next study.

Use of AI tools declaration

The author declares that no Artificial Intelligence (AI) tools were used in the creation of this article.

Acknowledgments

This research was funded by the Russian Science Foundation, project number 23-29-00108.

Conflict of interest

The author declares no conflict of interest.

References

1. Ehrmann A, Blachowicz T (2018) Systematic study of magnetization reversal in square Fe nanodots of varying dimensions in different orientations. *Hyperfine Interact* 239: 48. https://doi.org/10.1007/s10751-018-1523-1
2. Claridge SA, Castleman Jr AW, Khanna SN, et al. (2009) Cluster-assembled materials. *ACS Nano* 3: 244–255. https://oi.org/10.1021/nn800820e
3. Guo Y, Du Q, Wang P, et al. (2021) Two-dimensional oxides assembled by M_4 clusters (M = B, Al, Ga, In, Cr, Mo, and Te). *Phys Rev Res* 3: 043231. https://doi.org/10.1103/PhysRevResearch.3.043231
4. Bista D, Sengupta T, Reber AC, et al. (2021) Interfacial magnetism in a fused superatomic cluster $[Co_6Se_8(PEt_3)_5]_2$. *Nanoscale* 13: 15763. https://doi.org/10.1039/d1nr00876e
5. Bramwell ST, Gingras MJ (2001) Spin ice state in frustrated magnetic pyrochlore materials. *Science* 294: 1495–1501. https://doi.org/10.1126/science.1064761
6. Castelnovo C, Moessner R, Sondhi SL (2008) Magnetic monopoles in spin ice. *Nature* 451: 42–45. https://doi.org/10.1038/nature06433
7. Yumnam G, Guo J, Chen Y, et al. (2022) Magnetic charge and geometry confluence for ultra-low forward voltage diode in artificial honeycomb lattice. *Mater Today Phys* 22: 100574. https://doi.org/10.1016/j.mtphys.2021.100574
8. Keswani N, Singh R, Nakajima Y, et al. (2020) Accessing low-energy magnetic microstates in square artificial spin ice vertices of broken symmetry in static magnetic field. *Phys Rev B* 102: 224436. https://doi.org/10.1103/PhysRevB.102.224436
9. Belim SV, Lyakh OV (2022) Phase transitions in an ordered 2D array of cubic nanoparticles. *Lett Mater* 12: 126–130. https://doi.org/10.22226/2410-3535-2022-2-126-130
10. Valdés DP, Lima E, Zysler R, et al. (2021) Role of anisotropy, frequency, and interactions in magnetic hyperthermia applications: Noninteracting nanoparticles and linear chain arrangements. *Phys Rev Appl* 15: 044005. https://doi.org/10.1103/PhysRevApplied.15.044005
11. Li Y, Paterson GW, Macauley GM, et al. (2019) Superferromagnetism and domain-wall topologies in artificial "Pinwheel" spin ice. *ACS Nano* 13: 2213–2222. https://doi.org/10.1021/acsnano.8b08884
12. Fuentes-García JA, Diaz-Cano AI, Guillen-Cervantes A, et al. (2018) Magnetic domain interactions of Fe_3O_4 nanoparticles embedded in a SiO_2 matrix. *Sci Rep* 8: 5096. https://doi.org/10.1038/s41598-018-23460-w
13. Costanzo S, Ngo A, Russier V, et al. (2020) Enhanced structural and magneticproperties of fcc colloidal crystals of cobalt nanoparticles. *Nanoscale* 12: 24020–24029. https://doi.org/10.1039/D0NR05517D
14. Fedotova JA, Pashkevich AV, Ronassi AA, et al. (2020) Negative capacitance of nanocomposites with CoFeZr nanoparticles embedded into silica matrix. *J Magn Magn Mat* 511: 166963. https://doi.org/10.1016/j.jmmm.2020.166963

15. Kołtunowicz TN, Bondariev V, Zukowski P, et al. (2020) Ferromagnetic resonance spectroscopy of CoFeZr-CaF_2 granular nanocomposites. *Prog Electromagn Res M* 91: 11–18. https://doi.org/10.2528/PIERM19112107
16. Timopheev AA, Ryabchenko SM, Kalita VM, et al. (2009) The influence of intergranular interaction on the magnetization of the ensemble of oriented Stoner-Wohlfarth nanoparticles. *J Appl Phys* 105: 083905. https://doi.org/10.1063/1.3098227
17. Belim SV, Lyakh OV (2022) A study of a phase transition in an array of ferromagnetic nanoparticles with the dipole-dipole interaction using computer simulation. *Phys Metals Metallogr* 123: 1049–1053. https://doi.org/10.1134/S0031918X22601202
18. Nguyen MD, Tran HV, Xu S (2021) Fe_3O_4 nanoparticles: Structures, synthesis, magnetic properties, surface functionalization, and emerging applications. *Appl Sci* 11: 11301. https://doi.org/10.3390/app112311301
19. Köhler T, Feoktystov A, Petracic O, et al. (2021) Mechanism of magnetization reduction in iron oxide nanoparticles. *Nanoscale* 13: 6965–6976. https://doi.org/10.1039/D0NR08615K
20. Lemine OM, Madkhali N, Alshammari M, et al. (2021) Maghemite (γ-Fe_2O_3) and γ-Fe_2O_3-TiO_2 nanoparticles for magnetic hyperthermia applications: Synthesis, characterization and heating efficiency. *Materials* 14: 5691. https://doi.org/10.3390/ma14195691
21. Batlle X, Moya C, Escoda-Torroella M, et al. (2022) Magnetic nanoparticles: From the nanostructure to the physical properties. *J Magn Magn Mat* 543: 168594. https://doi.org/10.1016/j.jmmm.2021.168594
22. Lazzarini A, Colaiezzi R, Passacantando M, et al. (2021) Investigation of physico-chemical and catalytic properties of the coating layer of silica-coated iron oxide magnetic nanoparticles. *J Phys Chem Solids* 153: 110003. https://doi.org/10.1016/j.jpcs.2021.110003
23. Ovejero JG, Spizzo F, Morales MP, et al. (2021) Mixing iron oxide nanoparticles with different shape and size for tunable magneto-heating performance. *Nanoscale* 13: 5714–5729. https://doi.org/10.1039/D0NR09121A
24. Li Y, Baberschke K (1992) Dimensional crossover in ultrathin Ni(111) films on W(110). *Phys Rev Lett* 68: 1208. https://doi.org/10.1103/PhysRevLett.68.1208
25. Prudnikov PV, Prudnikov VV, Medvedeva MA (2014) Dimensional effects in ultrathin magnetic films. *Jetp Lett* 100: 446–450. https://doi.org/10.1134/S0021364014190096
26. Luis F, Bartolomé F, Petroff F, et al. (2006) Tuning the magnetic anisotropy of Co nanoparticles by metal capping. *Europhys Lett* 76: 142. https://doi.org/10.1209/epl/i2006-10242-2
27. Landau DP, Binder K (1978) Phase diagrams and multicritical behavior of a three-dimensional anisotropic heisenberg antiferromagnet. *Phys Rev B* 17: 2328. https://doi.org/10.1103/PhysRevB.17.2328
28. Binder K (1981) Critical properties from Monte-Carlo coarse-graining and renormalization. *Phys Rev Lett* 47: 693. https://doi.org/10.1103/PhysRevLett.47.693
29. Lisjak D, Mertelj A (2018) Anisotropic magnetic nanoparticles: A review of their properties, syntheses and potential applications. *Prog Mater Sci* 95: 286–328. https://doi.org/10.1016/j.pmatsci.2018.03.003
30. Aquino VRR, Figueiredo LC, Coaquira JAH, et al. (2020) Magnetic interaction and anisotropy axes arrangement in nanoparticle aggregates can enhance or reduce the effective magnetic anisotropy. *J Magn Magn Mat* 498: 166170. https://doi.org/10.1016/j.jmmm.2019.166170

31. Gallina D, Pastor GM (2021) Structural disorder and collective behavior of two-dimensional magnetic nanostructures. *Nanomaterials* 11: 1392. https://doi.org/10.3390/nano11061392
32. Gu E, Hope S, Tselepi M, et al. (1999) Two-dimensional paramagnetic-ferromagnetic phase transition and magnetic anisotropy in Co(110) epitaxial nanoparticle arrays. *Phys Rev B* 60: 4092. https://doi.org/10.1103/PhysRevB.60.4092
33. Benitez MJ, Mishra D, Szary P, et al. (2011) Structural and magnetic characterization of self-assembled iron oxide nanoparticle arrays. *J Phys Condens Matter* 23: 126003. https://doi.org/10.1088/0953-8984/23/12/126003
34. Spasova M, Wiedwald U, Ramchal R, et al. (2002) Magnetic properties of arrays of interacting Co nanocrystals. *J Magn Magn Mat* 240: 40–43. https://doi.org/10.1016/S0304-8853(01)00723-5
35. Schäffer AF, Sukhova A, Berakdar J (2017) Size-dependent frequency bands in the ferromagnetic resonance of a Fe-nanocube. *J Magn Magn Mat* 438: 70–75. https://doi.org/10.1016/j.jmmm.2017.04.065
36. Morgunov RB, Koplak OV, Allayarov RS, et al. (2020) Effect of the stray field of Fe/Fe_3O_4 nanoparticles on the surface of the CoFeB thin films. *Appl Surf Sci* 527: 146836. https://doi.org/10.1016/j.apsusc.2020.146836
37. Ren H, Xiang G (2021) Morphology-dependent room-temperature ferromagnetism in undoped ZnO nanostructures. *Nanomaterials* 11: 3199. https://doi.org/10.3390/nano11123199
38. Gao Y, Hou QY, Liu Y (2019) Effect of Fe doping and point defects (V_O and V_{Sn}) on the magnetic properties of SnO_2. *J Supercond Nov Magn* 32: 2877–2884. https://doi.org/10.1007/s10948-019-5053-0
39. Zhang C, Zhou M, Zhang Y, et al. (2019) Effects of oxygen vacancy on the magnetic properties of Ni-doped SnO_2 nanoparticles. *J Supercond Nov Magn* 32: 3509–3516. https://doi.org/10.1007/s10948-019-5094-4
40. Ming D, Xu L, Liu D, et al. (2008) Fabrication and phase transition of long-range-ordered, high-density GST nanoparticle arrays. *Nanotechnology* 19: 505304. https://doi.org/10.1088/0957-4484/19/50/505304
41. Vaz CAF, Bland JAC, Lauhoff G (2008) Magnetism in ultrathin film structures. *Rep Prog Phys* 71: 056501. https://doi.org/10.1088/0034-4885/71/5/056501